Prototype of a Quasi-Optical Launcher System of a 4 mm Round-Trip Interferometer for the QUEST Spherical Tokamak Experiments*)

Miu YUNOKI, Hiroshi IDEI[1)], Kazuo NAKAMURA[1)], Masaharu FUKUYAMA, Ryuichi ASHIDA, Daichi OGATA, Takumi ONCHI[1)], Ryuya IKEZOE[1)] and Masayuki YOSHIKAWA[2)]

Interdisciplinary Graduate School of Engineering Sciences, Kyushu University, Fukuoka 816-8580, Japan
[1)]*Research Institute for Applied Mechanics, Kyushu University, Fukuoka 816-8580, Japan*
[2)]*Plasma Research Center, University of Tsukuba, Ibaraki 305-8577, Japan*

(Received 9 January 2019 / Accepted 16 April 2019)

A launcher system for a round-trip interferometer, with a corrugated horn antenna and two quasi-optical mirrors, has been developed for the QUEST spherical tokamak experiment. The corrugated horn antenna has been designed using a three-dimensional (3D) electromagnetic simulator. At low power bench test, intensity and phase profiles at 0.1 m from antenna aperture show coaxial patterns as predicted by the 3D simulator, in agreement with the calculation results using an in-house developed Kirchhoff integral code. The designed waist sizes of the focused beam at a target position are 22 mm in the horizontal x direction and 43 mm in the vertical y direction. The beam reaches the target plate at QUEST's center-post and is reflected back along the line-of-sight round-trip. A well-focused beam of 32 and 36 mm in size (x, y) has been obtained at the target position. The HE_{11} mode excitation, beam transmission, and focusing properties are discussed for the prototype launcher system.

Keywords: QUEST, spherical tokamak, interferometer, electron density measurement, corrugated horn antenna, quasi-optical mirror, Gaussian beam

DOI: 10.1585/pfr.14.3402122

1. Introduction

The millimeter wave interferometer is a major diagnostic tool for measuring plasma electron density in nuclear fusion research. A new 4 mm heterodyne interferometer has been developed for the QUEST spherical tokamak experiments. The QUEST device is equipped with a hot first wall to control hydrogen recycling [1]. A complex water cooling system has been installed behind the hot wall and the flat-end plates. Vertical chords were not available for the interferometer setting in the vacuum vessel due to interferences with the flat top and bottom divertor-plates and the water cooling system.

Since the tangential chords with a magnetic axis in the plasma are substantially long, a line-of-sight round-trip was considered for the interferometer at the mid-plane. The proposed launcher system consists of three components, i.e., a corrugated horn antenna and two quasi-optical (QO) mirrors. The Gaussian beam, converted from an output HE_{11} mode of the corrugated horn antenna, is focused at the center-post target with two QO mirrors. The incident and reflected waves are sampled by three-port directional couplers at a stage prior to the launcher system. The reflected-wave phase is measured by contrasting it with the incident wave phase, after being transmitted twice through the plasma.

The corrugated horn antenna was designed with a three-dimensional (3D) electromagnetic simulator, using the software COMSOL Multiphysics. The performance of the horn antennas was verified in low-power test at Kyushu University facilities [2]. Because of limited space, we adopted the configuration using a two-mirror system so that the QO beam can be 99% transmitted for the interferometer. The two QO mirror surfaces were designed using a developed Kirchhoff integral code and Gaussian optics with a phase-matching concept [3]. A similar two-mirror launcher system has also been developed for the 28 GHz ECHCD and EC plasma ramp-up experiments at QUEST [4]. The total QO-transmission and focusing performances of the launcher system in the interferometer were also benchmarked with low-power tests.

In this paper, Sections 2 and 3 describe the development of the corrugated horn antenna and the two-mirror system, respectively. A summary is given in Section 4.

2. Development of the Corrugated Horn Antenna

The corrugated horn antenna has been widely used to excite a linearly polarized coaxial beam in various QO applications. In the corrugated horn antenna, a fundamental

author's e-mail: 2ES17232W@kyudai.jp, idei@triam.kyushu-u.ac.jp
*) This article is based on the presentation at the 27th International Toki Conference (ITC27) & the 13th Asia Pacific Plasma Theory Conference (APPTC2018).

circular TE°_{11} mode at the antenna input is transformed into the HE_{11} mode, polarized linearly at the antenna output. The amplitude profile of the HE_{11} mode is expressed as a 0-th order Bessel function J_0 similar to a Gaussian profile, and the curvature of the phase front depends on the open (half cone) angle of the antenna.

2.1 Design of the antenna

The corrugation parameters and profile of the antenna determine its performance. Figure 1 illustrates the coaxial series profile of the j-th corrugation slots, with top-radii a_j and depths d_j ($j = 1..., ..., N$), together with the a_i and a_o of the input and output aperture radii of the antenna, where N is the total number of the slots. The corrugation pitch and slot widths, p and w, are also shown in the figure. The antenna length L, is expressed as $L = (N-1)p + w$. A broadband antenna with operating minimum and maximum frequencies of $f_{max} = 75$ GHz and $f_{min} = 108.6$ GHz are considered here. Some of the antenna's corrugation parameters were selected along some design of the corrugated horn antenna [5], as shown in Table 1.

The first five corrugation slots from the input, of $j \le N_{mod}$ (= 5), were used for the incident TE°_{11} mode to be mode converted to the output HE_{11} mode. A mode-converter method with variable-depth slots was adopted. The corrugation depths d_j of $[N_{mod} < j \le N]$ should normally be equal to the quarter wavelength, except for the mode conversion section, but the depth d_j was considered as a function of the aperture radius a_j along with the designs. The input aperture radius of the antenna a_i was 1.59 mm, which is a fundamental circular waveguide size.

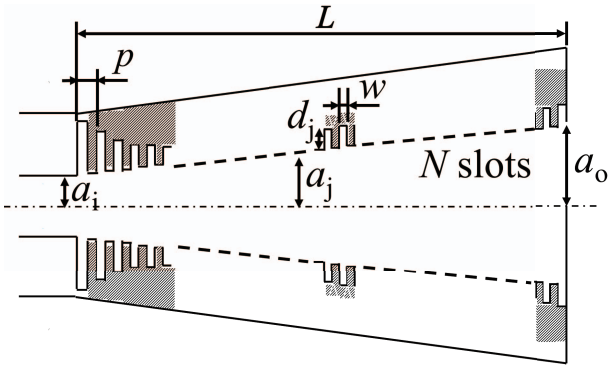

Fig. 1 Geometric parameters of the corrugated horn antenna.

Table 1 Design parameters of corrugated horn antenna.

Subject	Parameters
Aperture radii a_i, a_o [mm]	1.59, 8.60
Pitch and slot width p, w [mm]	0.67, 0.47
N, mode-converter slot number N_{mod}	60, 5
Depth d_j (j = 6, ... , 60) [mm]	0.89 - 0.74
Opened (half cone) angle [degree]	9.07

2.2 Simulated results and discussion on the designs

The radiation field was evaluated using a 3D electromagnetic model, using COMSOL, in the operating frequency of 75.09 GHz. The corrugation profile and parameters of the antenna listed in Table 1 were modeled using COMSOL, and the incident TE°_{11} mode was excited at the input to be transformed into the HE_{11} mode in the first five slots. Figures 2 (a) and (b) show the input and output field amplitudes indicated by arrows. The arrow size and direction express the magnitude and the polarized direction of the amplitude, respectively. The magnitudes are also indicated in the color mapping by means of arrows. The incident circular TE°_{11} mode is mainly polarized in the horizontal direction, but it is bent toward the normal direction to the waveguide wall because of zero tangential fields on the wall. The incident wave was correctly transformed into the HE_{11} mode, polarized horizontally at the output. A linear polarization was properly obtained at the output aperture.

The HE_{11} mode contents of the simulated complex field pattern were evaluated. The mode contents, C_{fg}, of a target complex amplitude $f(x,y)$ against the HE_{11} eigenmode $g(x,y)$ is written as [6],

$$C_{fg} = \frac{\left|\int f(x,y)g^*(x,y)\mathrm{d}x\mathrm{d}y\right|^2}{\int |f(x,y)|^2\mathrm{d}x\mathrm{d}y \cdot \int |g(x,y)|^2\mathrm{d}x\mathrm{d}y}, \quad (1)$$

where complex amplitudes are defined by the intensity $I(x,y)$ and phase $\Phi(x,y)$ profiles as $\sqrt{I(x,y)}\exp[j\,\Phi(x,y)]$. The target complex field $f(x,y)$ at the output aperture was interpolated from the grid field data in the COMSOL using

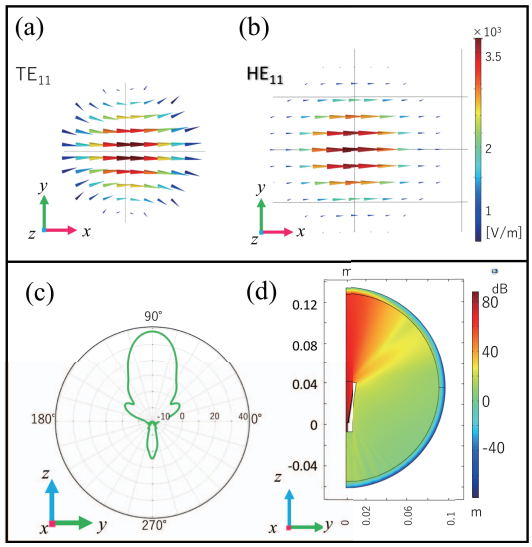

Fig. 2 (a) Input and (b) output field amplitude indicated by arrows. The arrow size and direction express the magnitude and polarized direction of the amplitude. The magnitudes are also indicated in the color mapping by means of arrows. (c) Directivity of the forward (FWD) and backward (BWD) components. (d) Radiation field pattern. Figures (c) and (d) are plotted in logarithmic scales.

the two dimensional (2D) cubic spline method. The mode contents of the expected HE_{11} mode in the simulated field was calculated as 0.94 by Eq. 1, indicating proper excitation of the HE_{11} mode at the antenna. The antenna was surrounded by perfect matching layers in the COMSOL modeling, and the forward (FWD) and backward (BWD) radiation fields were evaluated. Figures 2 (c) and (d) show the directivity of the FWD and BWD components, and the radiated amplitude pattern. Excellent directivity and radiation pattern, without noticeable side lobes, were also obtained in the COMSOL simulation.

2.3 Low-power antenna tests

2.3.1 Measurement system for low-power tests

The operating frequency was 75.09 GHz for the 4 mm interferometer. A schematic diagram of the measurement system is shown in Fig. 3. The fine frequency was selected to have low reflectance at a quartz vacuum window of 12 mm of thickness, as shown in Fig. 6 (a). The millimeter wave of the frequency was generated with a synthesizer output (3.128750000 GHz) and two active-frequency doublers and an six times active-frequency multiplier. The 75 GHz wave generated was fed to the corrugated horn antenna via a transducer and a WR10 directional coupler. Here, a conventional transducer from fundamental WR10 rectangular to circular waveguides was also used. The propagating wave from the corrugated horn antenna was measured for heterodyne detection, using a sixth harmonic mixer. A local oscillator wave (12.526666667 GHz) generated by the synthesizer (3.131666667 GHz) and two active doublers were used for the heterodyne detection, and the intermediate-frequency wave of 70 MHz was measured using a network analyzer. The two synthesizers were phased-locked with a 10 MHz reference wave. Band-pass and high-pass filters were used to reject unwanted harmonic components from the doubler. The intensity ratio and phase difference between the propagating and reference waves were detected at the analyzer. The reference wave was sampled at the directional coupler installed before the corrugated horn antenna. A 3D stage controlled by a PC was set in front of the corrugated horn antenna, or the launcher system, when measuring the propagating beam profile.

2.3.2 Radiated-field measurement results and discussion

The intensity and phase profiles of the beam radiated from the antenna were measured at a propagating distance z of 0.1 m. In the antenna test, the vertical electric field was excited and measured. Figure 4 shows the measured intensity and phase contour plots, indicating the coaxial Gaussian-like intensity and parabolic phase patterns. Here, the x and y coordinates (horizontal and vertical directions) are perpendicular to the propagating direction, z.

The measured radiation profiles on the x and y axes

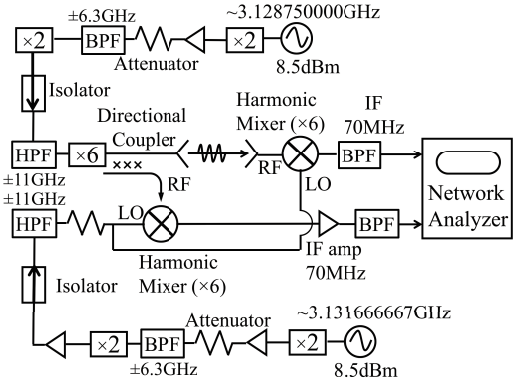

Fig. 3 Schematic diagram of 75 GHz low-power test facilities.

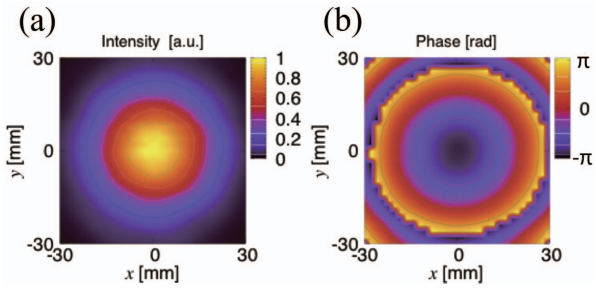

Fig. 4 Measured (a) intensity and (b) phase patterns of the corrugated horn antenna at a propagating distance z = 0.1 m.

are compared with those computed in the COMSOL simulation and calculated using a developed Kirchhoff integral code. The Kirchhoff integral of the radiation field E^{rad} is expressed as [6]:

$$E^{\mathrm{rad}}(x,y,z) = \frac{1}{4\pi}\int\int E(x_2,y_2)\frac{\exp(-jk_0r)}{r} \times\left(jk_0+\frac{1}{r}\right)\frac{z}{r}\mathrm{d}x_2\mathrm{d}y_2, \quad (2)$$

$$r = \sqrt{(x-x_2)^2+(y-y_2)^2+z^2}, \quad (3)$$

where (x, y, z) and (x_2, y_2) are the coordinates of the radiation point and of the antenna output aperture, with a coordinate origin at the center of the aperture. The integral range is within the aperture radius a_0. The aperture field E (x_2, y_2) was interpolated from the COMSOL grid data using the cubic spline method, and was integrated inside the aperture.

Figure 5 shows the intensity and phase profiles on the x and y axes, measured at low-power level, simulated using COMSOL, and evaluated using the Kirchhoff integral, at the propagation distance z = 0.1 m. The measured intensity and phase profiles are in good agreement with the simulation results. The Kirchhoff integral results agreed well with the measured and COMSOL simulated data, although a remark should be made: in the irradiant beam-profiles shown in Fig. 5, measured and COMSOL results contain diffraction but results for the Kirchhoff integral not.

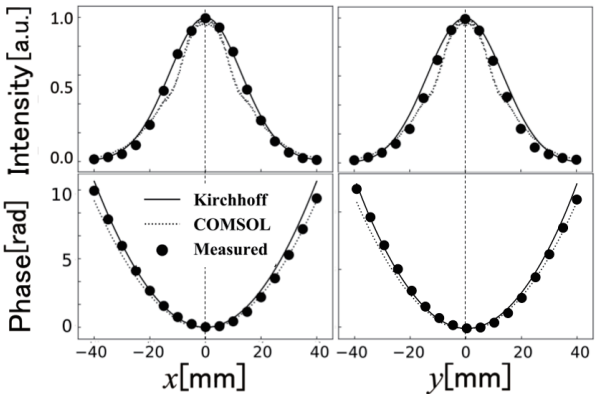

Fig. 5 Measured intensity and phase profiles in horizontal x and vertical y axes, along with the COMSOL and Kirchhoff integral code calculations at a propagating distance $z = 0.1$ m.

3. Development of a Two-Mirror Launcher System

A two-mirror launcher system was required to focus the beam on the center-post for the round-trip interferometer, as mentioned in Section 1. The center-post was boarded up with small stainless-steel flat plates of 70 mm in width and 170 mm in height. If the waist position of the beam, z_0, can be placed on a flat plate at the center-post, the beam can be correctly received by the same optics for the injection. The two-mirror launcher (and receiver, in a sense) system is a key component in the round-trip interferometer, together with the corrugated horn antenna.

3.1 Design of the launcher

First, geometrical mirror sizes should be considered for the launcher system to be installed in limited spaces. The mirror size should be larger than $3w$. Here w is the beam size in Gaussian optics [7] at the mirror. When the size is larger than $3w$, beam intensity of more than 99% can be covered [8]. The waist sizes w_{0x} of 22 mm and w_{0y} of 43 mm were chosen on the target plate to provide the $3w$ sizes at the center-post plate in the x (width) and y (height) directions, respectively. The second mirror size of $3w$ was evaluated by propagation analysis from the center-post to the mirror, in Gaussian optics. The beam radiated from the corrugated horn antenna must be correctly transmitted to the second mirror. The first mirror position affects the beam transmission function. The incident angle to the mirror should be considered to be as small as possible in order to reduce asymmetry at the beam center in the beam steering direction. If the first mirror position is too far from the corrugated horn antenna, the first mirror would be larger in size to attain 99% transmission, whereas the incident angle to the mirror would be smaller. The mirror edges sometimes have interferences on the transmission, depending on the mirror configuration. The position and size of the first mirror were determined in order to attain 99% transmission with a smaller incident angle to the mirror. Figure 6 shows the two-mirror configuration of the final launcher system in the design work, along with the target.

The irradiant beam from the antenna would be expanded to obtain a larger beam for focusing onto the target center-post plate by the second mirror. The irradiant HE_{11} mode phase front at the first mirror was converted into a Gaussian beam phase front to achieve the designed expanding beam to the second mirror. The propagating phases before and after the first mirror reflection were evaluated using the Kirchhoff integral and Gaussian optics, respectively, and the first mirror surface was designed using a developed, phase-matching code with the Kirchhoff integral. The phase front of the expanded Gaussian beam at the second mirror would be converted into a designed Gaussian-focusing beam with w_{0x} and w_{0y} at the target plate. The second mirror surface was designed using a similar phase-matching code using only Gaussian optics.

The designed mirror height contour plots of the first and second mirrors (M1 and M2) are also shown in Figs. 6 (b) and (c). The mirror height profiles are asymmetric in the beam steering x_m direction, as expected, particularly at M2. The mirror coordinates (x_m, y_m) are illustrated in the figure. Since strong focusing is required in the x direction (width) of the target center-post plate, the beam should be further expanded in this direction with the convex mirror curvature toward the second mirror. The first mirror surface was saddle shaped, or a hyperbolic paraboloid structure; *i.e.*, it was concave and convex in the x_m and y_m directions in order to obtain the different expanding properties in two directions, respectively, with asymmetry in the x_m direction. The second mirror surface was an elliptical paraboloid structure with relatively strong asymmetry in the x_m direction. A photograph of the two aluminum-mirror system fabricated is shown in Fig. 6 (d).

3.2 Low-power tests on the launcher and discussion

The launcher performance was verified at the low-power test facilities described in Section 3.1. The receiver of a sixth harmonic mixer with a fundamental WR10 waveguide was set at the target plate position where it is 1.354 m away from the M2, as illustrated in Fig. 6 (e). Figure 7 shows the intensity and phase contour plots of the focused beam measured at $z = 1.354$ m. The vertically elongated rectangular frames are shown as the target center-post plate area in the figure. Here, the beam fields were measured without the quartz window shown in Fig. 6 (a). The detailed effect of the quartz window on the beam focusing will be a topic of discussion for a future work, although a less effect has already been verified by our measurements.

In the launcher test, the horizontal field E_x was excited to demonstrate the O-mode operation of the interferometer in QUEST. The beam was accurately focused on the target plate with a relatively flat-phase front. Figure 8 shows

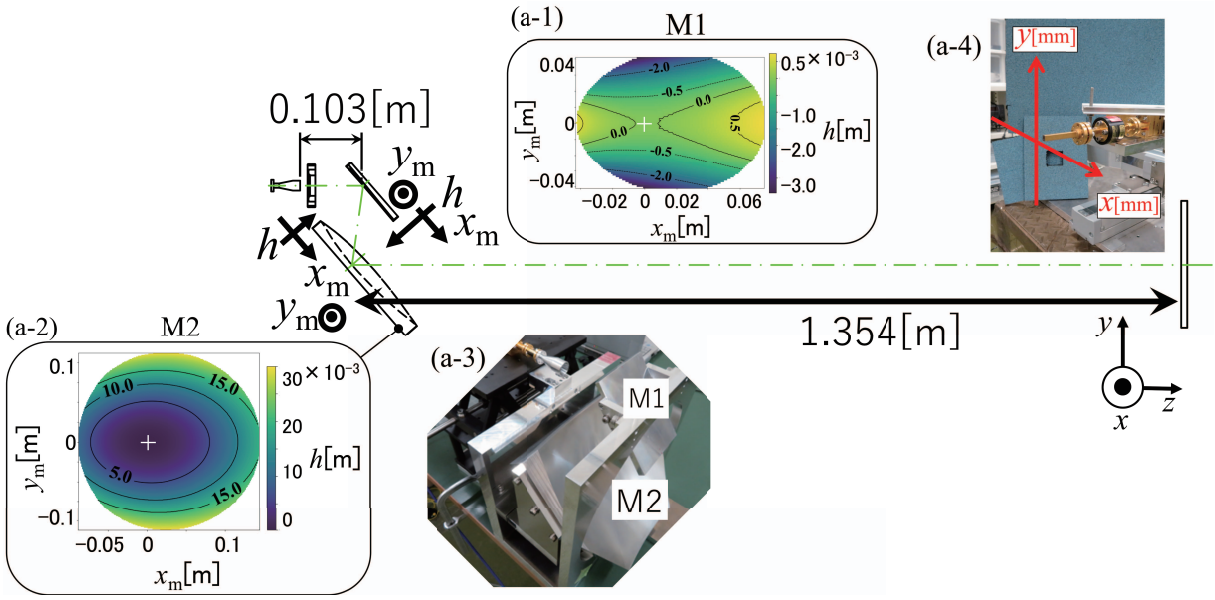

Fig. 6 (a): Launcher configuration with a focusing target. (b) and (c): Designed height h contour plots on the first and second (M1 and M2) mirror surfaces. The mirror coordinates (x_m, y_m) are illustrated in the figure. Photographs of (d): fabricated, aluminum M1 and M2 QO mirrors and (e): receiver for the low-power test. A quartz vacuum window of 12 mm in thickness is also shown in (a).

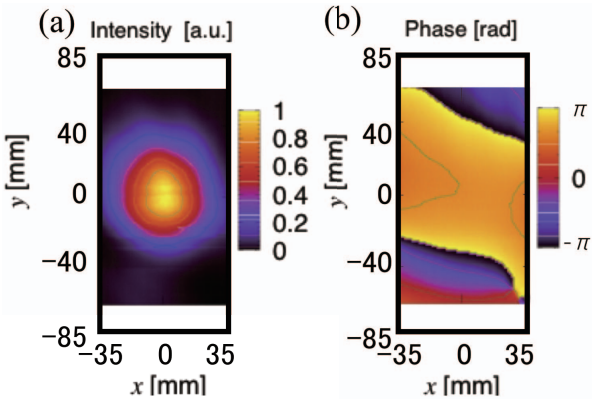

Fig. 7 Measured intensity and phase contour plots at the target of propagation position z = 1.354 m from the second mirror. Vertically elongated, rectangular frames show the target center-post plate area of 70 mm × 170 mm.

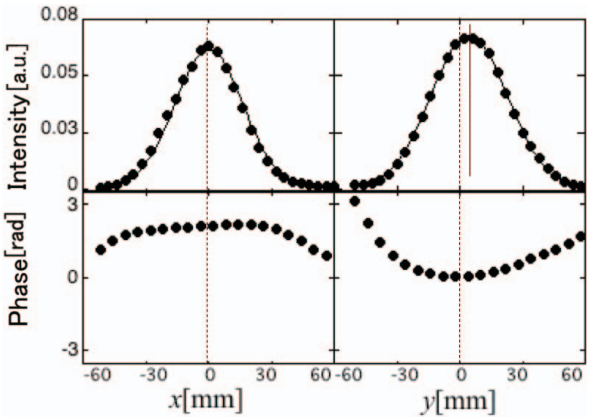

Fig. 8 Measured intensity and phase profiles on the horizontal x and vertical y axes.

the intensity and phase profiles on the x and y axes. The beam sizes w_x and w_y in the x and y directions were 32 and 36 mm, whereas the designed sizes were 22 and 43 mm, the same as the waist sizes, respectively. The beam was focused almost within the target plate, as shown in Fig. 7. The covered contents of the focused beam within the plate were evaluated as being 0.97 from the 2D integral of the intensity pattern within a plate of 70 mm × 170 mm.

Since the phase x profile is rather flat, the target position was close to the waist in the x direction. The beam expanded slightly in the y direction, which was suggested from the phase y profile. The beam is rather large and small in the x and y, directions, respectively. The narrow phase profile evaluated using the Kirchhoff integral in Fig. 5 might affect the focusing property, slightly differing from the design. The first mirror position of z = 0.103 was very close to the propagation position of z = 0.1 m in Fig. 5. Again, the Kirchhoff integral used for the mirror surface design did not include the diffraction effect. The Kirchhoff integral using the complex amplitude following some propagation will be used to include the diffraction effect for better focusing. The modified design and verification of its performance remain to be studied in future works.

4. Summary

The launcher system of the round-trip interferometer composed of a corrugated horn antenna, and two QO mirrors have been developed for the QUEST spherical toka-

mak experiments. The corrugated horn antenna was considered along the designs and COMSOL simulation. The proper HE_{11} mode beam excitation was confirmed in the simulations. The coaxial intensity and phase patterns were obtained at a propagating distance of $z = 0.1$ m in the low-power tests. These profiles matched considerably well with the COMSOL simulations. The Kirchhoff integral results agreed well with the measurement and simulations.

The two-mirror configuration was considered in order to attain 99% of transmission with a smaller incident angle to the mirrors. The mirror surfaces were designed using a Kirchhoff integral code and Gaussian optics along with the phase-matching concept. The well-focused beam, with beam sizes of $w_{0x} = 32$ mm and $w_{0y} = 36$ mm, was obtained at the target position in the low-power tests. The designed sizes were 22 and 43 mm, the same as the waist sizes. The covered contents of 97% within the target plate were attained for the focused beam. For better focusing, the Kirchhoff integral using complex amplitude following some propagation, including the diffraction effect, will be used to determine the mirror surfaces in future works.

Acknowledgment

This work was partially supported by the NIFS13KUDR085.

[1] K. Hanada *et al.*, Nucl. Fusion **57**, 126061 (2017).
[2] H. Idei *et al.*, Nucl. Fusion **46**, 489 (2006).
[3] S. Kubo *et al.*, Fusion Eng. Des. **26**, 319 (1995).
[4] H. Idei *et al.*, Fusion Eng. Des., accepted for publication (2019).
https://doi.org/10.1016/j.fusengdes.2019.02.027
[5] C.D. Granet and G.L. James, IEEE Antennas Propag. Mag. **47**, 76 (2005).
[6] H. Idei *et al.*, J. Infrared Millim. Terahertz Waves **36**, 662 (2015).
[7] Amnon Yariv, *Quantum Electronics* (John Wiley Sons Inc., 1975).
[8] M. Sakaguchi *et al.*, Plasma Fusion Res. **8**, 1405163 (2013).